Microwave Imaging: Research in Alternative Medical Imaging Modalities

Vinh Ngoc Nguyen

Wednesday, April 26, 2006

Abstract

Microwave imaging is an alternate breast cancer detection technique that uses microwaves to generate images based on differences in permittivity and conductivity. The large differences in permittivity and conductivity between normal and malignant breast tissue should allow for more reliable detection of breast cancer as opposed to conventional X-ray techniques.

This project aims to develop a 3-D microwave imaging system that utilizes microwaves for breast cancer detection.

To date, 3-D microwave imaging hardware has been developed for use in breast cancer detection. This hardware incorporates folded patch antennas, acetone/isopropyl alcohol matching fluid, an RF multiplexer switching system, and C++-based control software. Testing has shown that the hardware exhibits good system stability and Signal to Noise Ratio (SNR). However, an image has not yet been successfully reconstructed from measurements made using the microwave imaging hardware.

Future work will involve the assembly of a new hardware system for microwave imaging that addresses many of the flaws discovered in the current microwave imaging hardware. This system will operate in the gigahertz range and will utilize a new RF switching system, simple patch antennas, and a new imaging chamber design. It is anticipated that a functional microwave imaging system will be completed by Fall 2006.

1 Introduction

Breast cancer is the leading cause of death in women between 40 and 55 years of age [1]. The American Cancer Society estimates that 211,240 new cases of breast cancer were diagnosed in the United States in 2005 alone [2]. It also estimates that 40,870 deaths will have occurred due to breast cancer in 2005 [2]. Early detection of breast cancer has been shown to result in a 5-year survival rate of 96% [1].

The most popular imaging modality in use today for breast cancer screening and diagnosis is X-ray mammography [3]. While X-ray mammography offers high image resolution, it also possesses significant drawbacks. X-ray mammography has difficulty detecting tumors at their earliest stages [3]. It is also less effective at detecting tumors in women with dense breasts and in detecting tumors near the underarm or chest wall [3]. Conventional X-ray mammography also suffers from a low level of specificity between benign and malignant tissues [3]. This often results in high false-positive rates [3]. In addition, X-ray mammography utilizes ionizing radiation and thus may cause cellular damage [3]. Finally, X-ray mammography requires that the patient undergo painful chest compression [3].

Microwave imaging uses the differences in permittivity and conductivity between different tissues to reconstruct images. At frequencies in the neighborhood of 800 MHz, the permittivity of cancerous tissue is 3.75 times that of normal breast tissue while the conductivity is 6.75 times that of normal tissue [3]. The contrast between normal and cancerous breast tissue in conventional

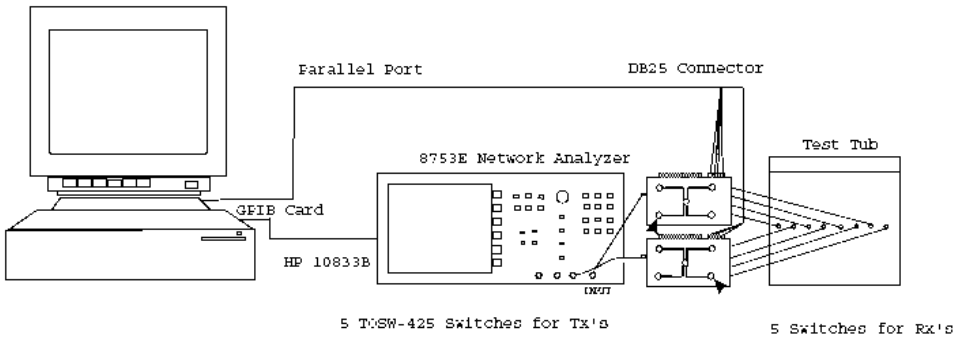

Figure 1: System Diagram [4]

X-ray mammography is on the order of 5%. Microwave imaging does not use ionizing radiation so there is a significantly reduced probability of causing cellular damage. Finally, microwave imaging does not require uncomfortable chest compressions.

2 Concept

The body part to be imaged is first placed in an imaging chamber lined with transmitting and receiving antennas. The chamber is then filled with a matching fluid whose electrical properties are matched to healthy tissue. A signal generated by a vector network analyzer is transmitted into the chamber via a selected transmitting antenna. This signal is received by a selected receiving antenna. The network analyzer than calculates an S21 value for the antenna combination based on the magnitude of the received signal relative to the transmitted signal. An RF switching system is used to measure S21 values for all antenna combinations. These S21 values are normalized relative to measurements made with only the matching fluid present. This permits the scattered field due to the differences in permittivity and conductivity in the chamber to be calculated. The collected S21 values are input into inversion software to reconstruct images of the permittivity and conductivity distributions of the imaging chamber contents. A diagram of a basic microwave imaging system is shown in Figure 1.

3 Prior Work–2-D Microwave Imaging System

Previous research into microwave imaging at Duke University had previously resulted in the development of a prototype 2-D microwave imaging system (Figure 2). This system utilized a cubic imaging chamber surrounded by 20 patch antennas configured to operate as 4 transmitting antennas and 16 receiving antennas. Each of the four vertical sides of the imaging had one transmitting

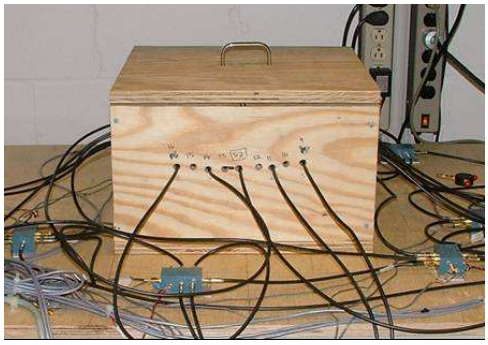

Figure 2: 2-D Microwave Imaging System

antenna and 4 receiving antennas placed up against it. The patch antennas all had an operating frequency of 1.5 GHz. Minicircuits TOSW-425 reflective multiplexers were used to switch between selected antennas. The multiplexers and the network analyzer were controlled using LabVIEW-based control software. The 90% Eucerin, 10% mineral oil, and 0.4 g/mL NaCl matching fluid described in [5] was used in the 2-D microwave imaging system. Considerable difficulty was encountered in attempting to reconstruct an imaging using measured data obtained from the 2-D imaging system. It was hypothesized that much of this difficulty could be attributed to design flaws in the 2-D imaging system. Considering the effort that would be needed to correct the flaws in the 2-D system, the decision was made to halt work on the 2-D system in favor of moving onto a 3-D imaging system.

4 3-D Microwave Imaging System

A prototype 3-D microwave imaging system was developed. The system consisted of a cubic imaging chamber surrounded by 100 folded patch antennas configured to operate as 44 transmitting antennas and 56 receiving antennas. These antennas were fabricated in 4 5-by-5 antennas arrays using multilayer Printed Circuit Boards (PCBs). 11 antennas in each panel were designated as transmitting antennas while 12 antennas in each panel were designated as receiving antennas. The folded patch antennas possessed a common operating frequency of 942 MHz. In addition, Minicircuits GSWA-4-30DR absorptive multiplexers were used to switch between antennas. The Eucerin/mineral oil-based matching fluid used in the 2-D microwave imaging system was replaced by an acetone/isopropyl alcohol matching fluid. Finally, the LabVIEW based control software used to control the 2-D system was replaced by C++-based control software in the 3-D imaging system.

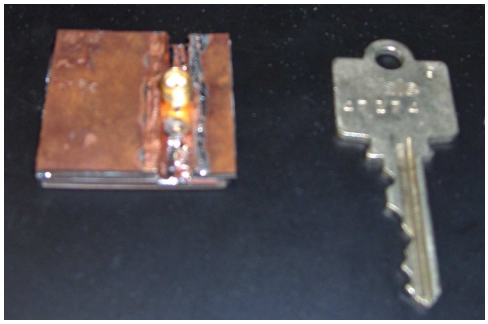

Figure 3: "Proof of concept" folded patch antenna

4.1 Imaging Chamber

The imaging chamber was an 18 cm by 18 cm by 18 cm cube formed by attaching the antenna panels together along their edges using 2-part epoxy adhesive. For use with the matching fluid, the chamber was lined with plastic sheeting to protect the antennas from the matching fluid.

4.2 Folded Patch Antennas

The antennas used in the 3-D microwave imaging system were selected to meet the two objectives of operating in the neighborhood of 800 MHz (where maximum contrast between normal and malignant mammary tissue exists) and of possessing a small antenna form factor. Based on these considerations, folded patch antennas were selected as the antenna to be used in the 3-D microwave imaging system.

4.2.1 Antenna Prototyping using CNC Milling Machine

A large form factor "proof of concept" folded patch antenna (Figure 3) was constructed using copper-clad FR-4 circuit boards and a CNC milling machine (Figure 4). Tests conducted using an HP 8753E vector network analyzer revealed good agreement between measured antenna performance and simulated antenna performance obtained using Ansoft HFSS.

4.2.2 Multilayer Printed Circuit Board Folded Patch Antennas

Based on difficulties encountered in manufacturing a prototype folded patch antenna using the CNC milling machine, it was decided to fabricate the imaging system's folded patch antennas in panels using multilayer Printed Circuit Boards (PCBs) (figure 5). Unfortunately, measured antenna performance (figure 6) for the multilayer PCB antennas was considerably worse than the simulated results obtained using both Ansoft HFSS and ECT (a proprietary simulation program) (figure 7). In addition, measured results indicated that the fabricated antennas

Figure 4: CNC milling machine

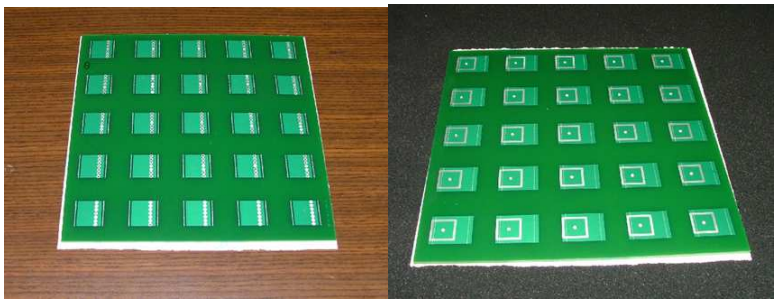

Figure 5: Unconnectorized multilayer PCB folded patch antenna panel

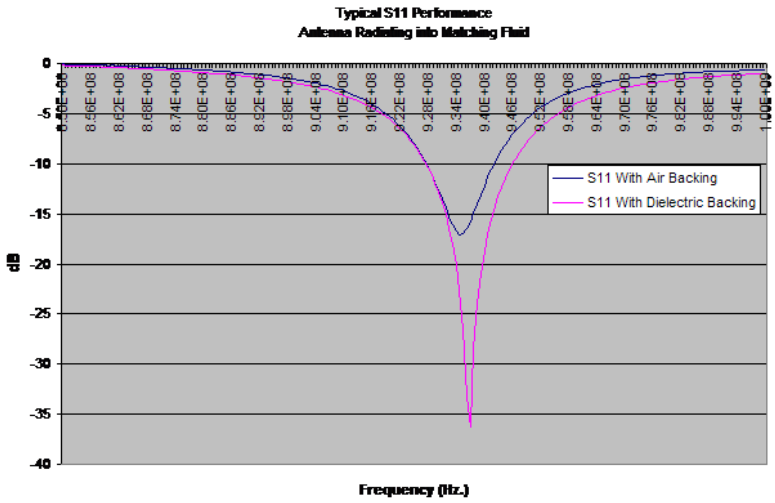

Figure 6: Measured antenna performance (S11)

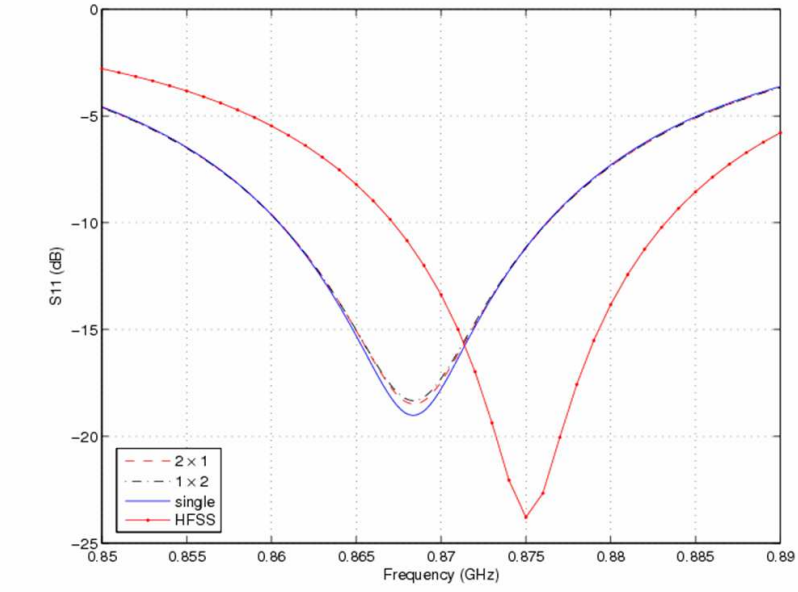

Figure 7: Simulated antenna performance (S11)

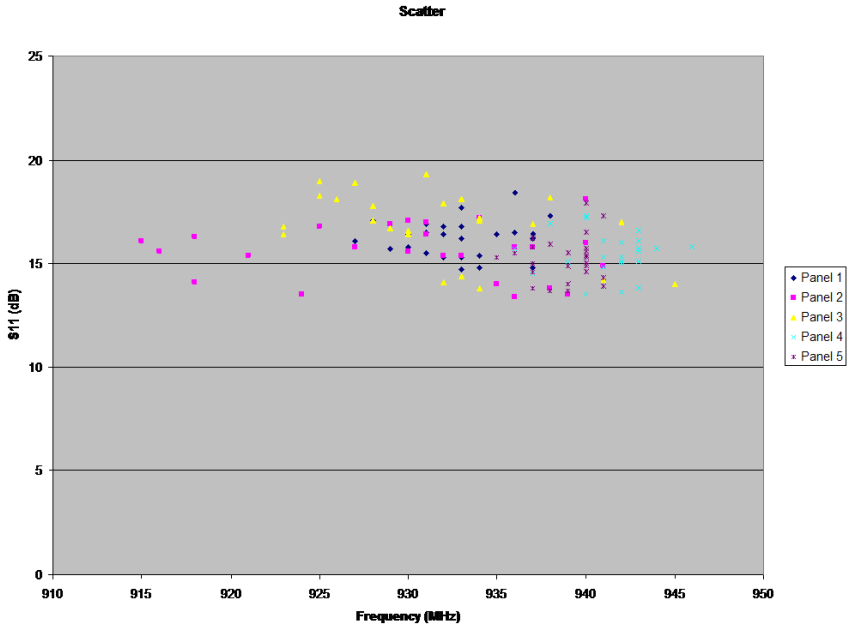

Figure 8: Center frequencies of all fabricated multilayer PCB patch antennas before tuning

were operating over a wide range of frequencies (figure 8). However, it was discovered that the antennas' operating frequencies could be tuned to a higher frequency by applying differing amounts of copper tape to the backside of each antenna to extend the antenna ground plane. Copper tape was used to tune all of the imaging chamber's antennas to a common operating frequency of 942 MHz.

4.3 RF Multiplexers

Experience with the 2-D microwave imaging system had shown that using absorptive RF multiplexers to switch between antennas was preferable to using reflective RF multiplexers. In the 2-D system, the reflective multiplexers would short unselected antennas to ground. This resulted in the signal emitted by the selected transmitting antenna reflecting off of the surrounding unselected antennas. The resulting reflected signals were not accounted for in the model used by the image reconstruction software. This most likely inhibited the reconstruction of an image using the 2-D microwave imaging system.

To attempt to improve upon the 2-D system, 1x16 (figure 10) and 1x4 (figure 11)RF multiplexer circuit boards were designed and built for use in the 3-D system. These boards used Minicircuits GSWA-4-30DR SP4T absorptive

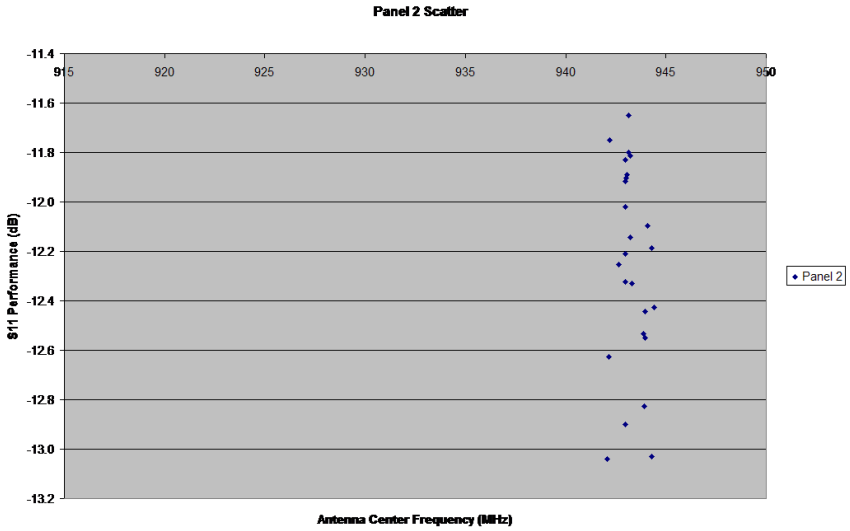

Figure 9: Center frequencies of all antennas on panel 2 after tuning

RF multiplexer chips to switch between RF channels. These RF multiplexer circuit boards were then assembled into an RF switching system (figure 12) . The system allowed the input and output ports of an HP8753E vector network analyzer with attached HP85046A S-parameter test kit to be switched between the transmitting and receiving antennas.

4.4 Control Software

To attempt to improve measurement times, C++ control software was developed to control the imaging hardware. The C++ control software had an average measurement time of 1 minute, 18 seconds as opposed to the LabVIEW

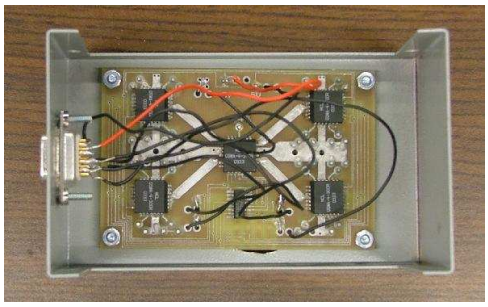

Figure 10: 1x16 RF multiplexer circuit board

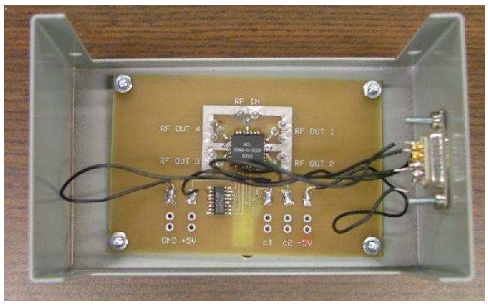

Figure 11: 1x4 RF multiplexer circuit board

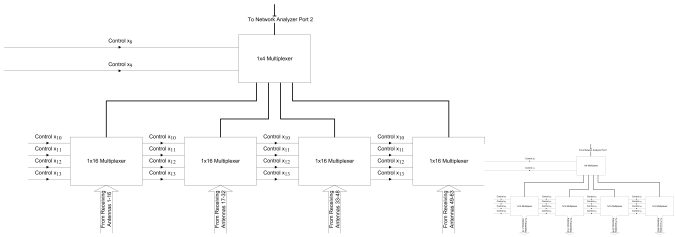

Figure 12: Block diagram of RF switching system

control software's average measurement time of 13 minutes, 16.8 seconds. It was determined that the main reason for the measurement time disparity was the fact that the LabVIEW control software was reinitializing the network analyzer before making each measurement. Disabling this portion of the LabVIEW control software resulted in measurement times of the same order as those obtained using the C++ control software.

5 Results

The assembled 3-D microwave imaging system was tested to determine the system stability and to determine the Signal-to-Noise ratio for several test objects.

5.1 System Stability

5.1.1 Test Procedure

The imaging chamber was filled with the acetone/isopropyl alcohol matching fluid. S21 measurements of all possible transmitter and receiver combinations were made with only the matching fluid in the chamber. Four additional measurement sweeps of all possible antenna combinations were made for a total of five measurement sweeps. Normalized S21 values were then calculated from the S21 measurements using Equation 1.

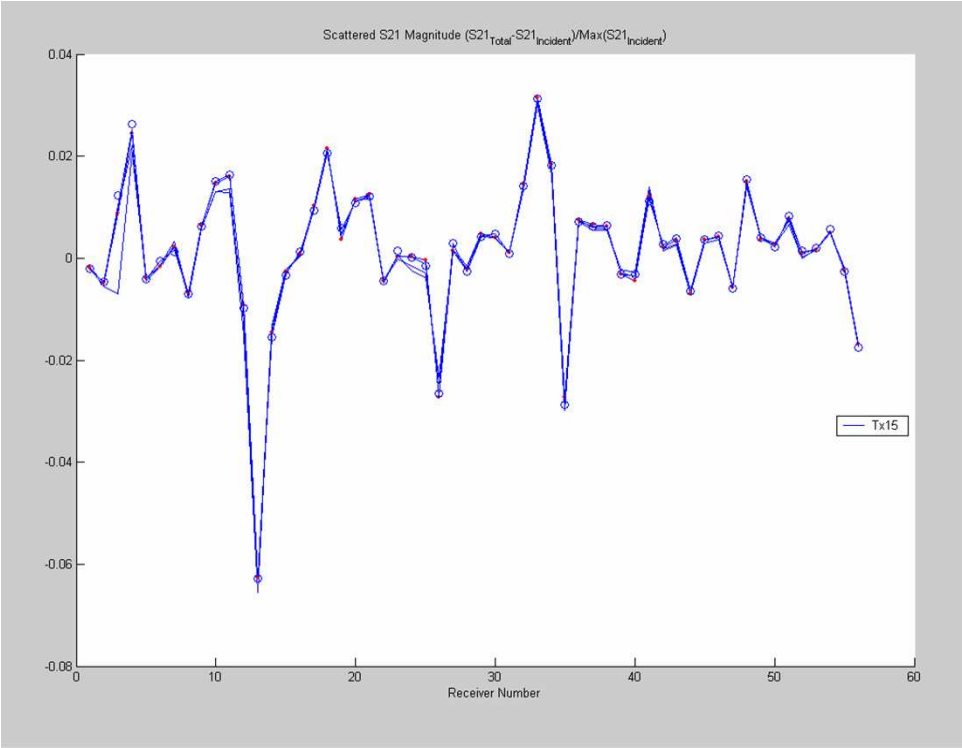

Figure 13: System stability

$$S_{21_{Norm}} = \frac{S_{21_{Total}} - S_{21_{Incident}}}{Max(S_{21_{Incident}})} \quad (1)$$

These normalized S21 values were then plotted and compared to determine the system stability. The results from all five measurement sweeps were then compared to determine the system's stability.

5.1.2 Test Results and Analysis

The results show close agreement from sweep to sweep (figure 13). This indicates a high degree of system stability.

5.2 Signal to Noise Ratio

5.2.1 Test Procedure

The imaging chamber was filled with the matching fluid. A background sweep consisting of S21 measurements of all possible antenna combinations was then made with only the fluid present in the imaging chamber. A target object was

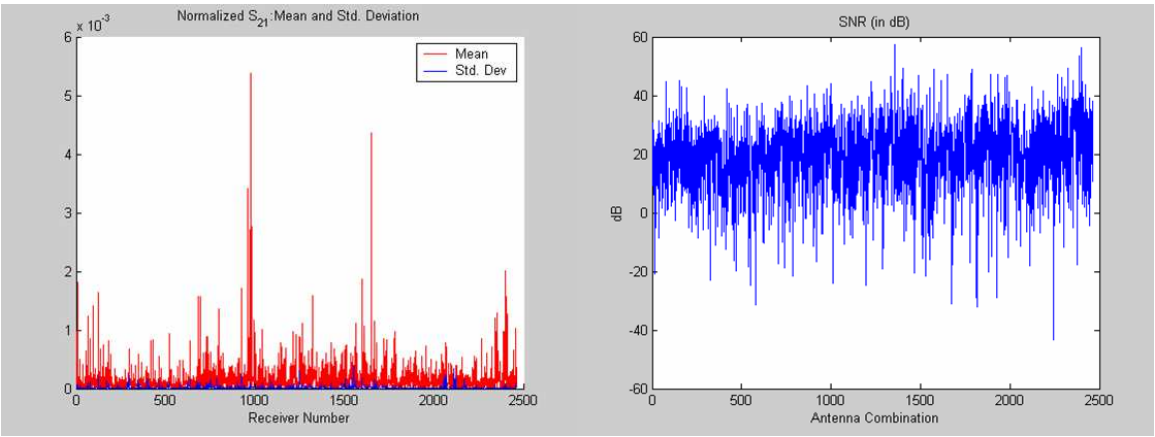

Figure 14: Signal to Noise Ratio for a 7 cm diameter water-filled balloon

then suspending in the imaging chamber using a thin cotton thread. An object sweep consisting of S21 measurements of all possible antenna combinations was then made with the target object present in the chamber. The normalized S21 and Signal to Noise Ratio (SNR) were then calculated for all combinations of transmitting and receiving antennas using Equation 1 and Equation 2.

$$SNR = 20log_{10}(\frac{\bar{x}}{\sigma}) \tag{2}$$

where the signal is defined as the mean of the normalized S21 values for a series of n measurements

$$signal = \bar{x} = \frac{1}{n}\sum_{i=1}^{n} x_i \tag{3}$$

and the per-channel noise is defined as the standard deviation

$$noise = \sigma = \sqrt{\frac{1}{n}\sum_{i=1}^{n}(x_i - \bar{x})^2} \tag{4}$$

5.2.2 Test Results and Analysis

The Signal to Noise Ratio (SNR) test was conducted for a roughly spherical water-filled balloon with a diameter of 7 cm (figure 14), a water-filled balloon with a diameter of 4 cm (figure 15), a water-filled balloon with a diameter of 1.5 cm (figure 16), and a water-filled plastic cylinder with a diameter of 4 cm and a height of 4 cm (figure). The SNR values were all significantly above 0 dB for most channels for all targets. This indicates that the measured signal is greater than the measured noise for most antenna combinations.

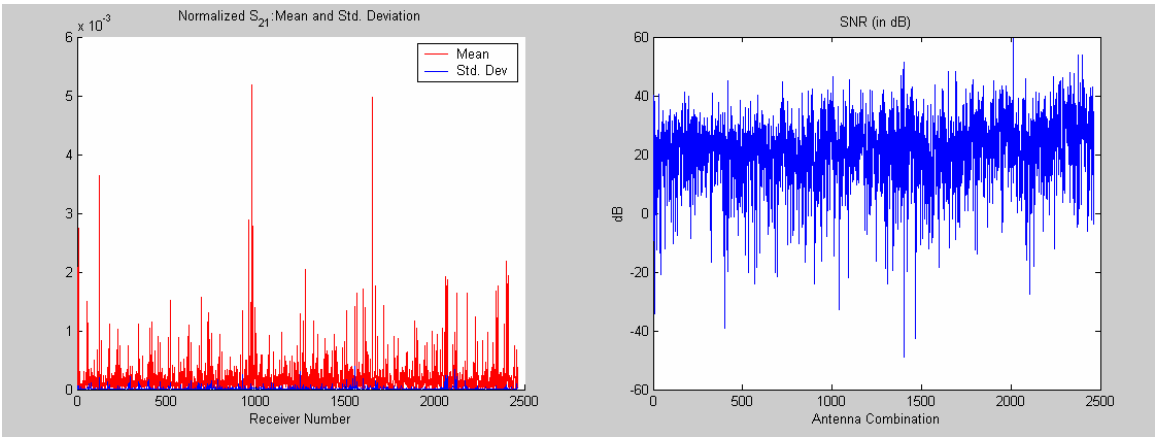

Figure 15: Signal to Noise Ratio for a 4 cm diameter water-filled balloon

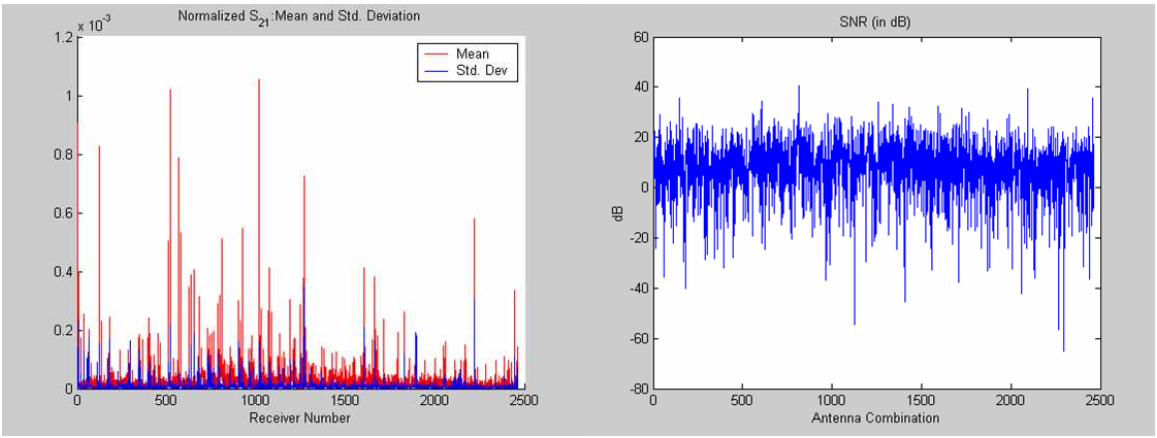

Figure 16: Signal to Noise Ratio for a 1.5 cm diameter water-filled balloon

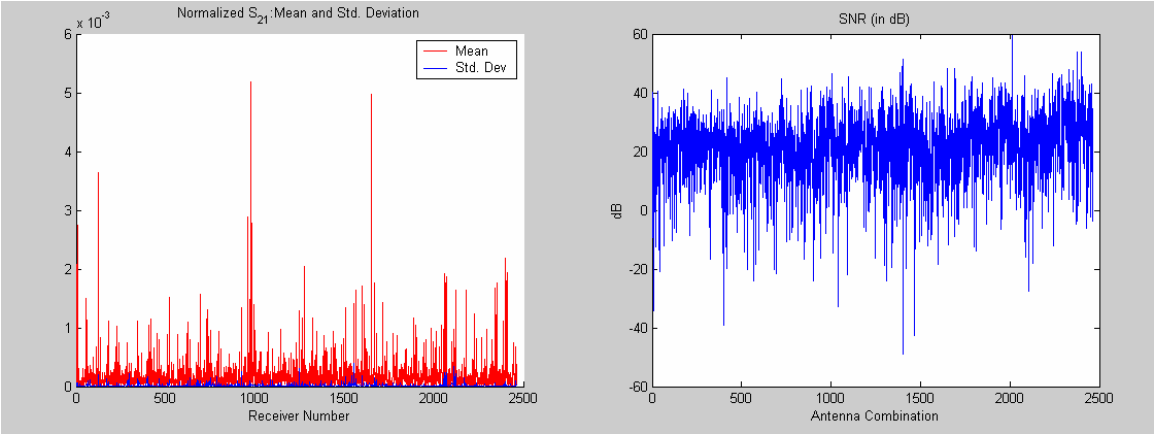

Figure 17: Signal to Noise Ratio for a water-filled plastic cylinder with 4 cm diameter and 4 cm height

6 Conclusion

The hardware for a 3-D microwave imaging system was developed. Testing revealed that the system exhibited good stability and good SNR. However, an image had not yet been successfully reconstructed from measurements made using the 3-D microwave imaging hardware.

The inability to reconstruct an image from measured data could be due to any out of several possible causes. The SNR of the measurements may have been insufficient to successfully reconstruct an image. This could be due to attenuation due to the multiplexers. This could also be due to insufficient scattered signal given the large wavelength of the transmitted signal compared to the small target objects. In addition, the configuration of the antenna panels and the imaging chamber could have resulted in ringing due to transmitted waves reflecting off of either the imaging chamber walls or the antenna panels. Finally, the inability to successfully reconstruct an image could stem from inadequate modeling of the complex folded patch antenna shape in the inversion software used to reconstruct images.

7 Future Work

Future work will be focused on developing a second 3-D microwave imaging system. This system will be designed to avoid many of the flaws in the current 3-D microwave imaging system. The proposed 3-D microwave imaging system will incorporate angled antenna panels to reduce reflections within the imaging chamber. It will also operate at a higher frequency (around 2.45 GHz) than the current imaging system to increase the scattered signal off of target objects. This higher operating frequency will also permit simple patch antennas to be

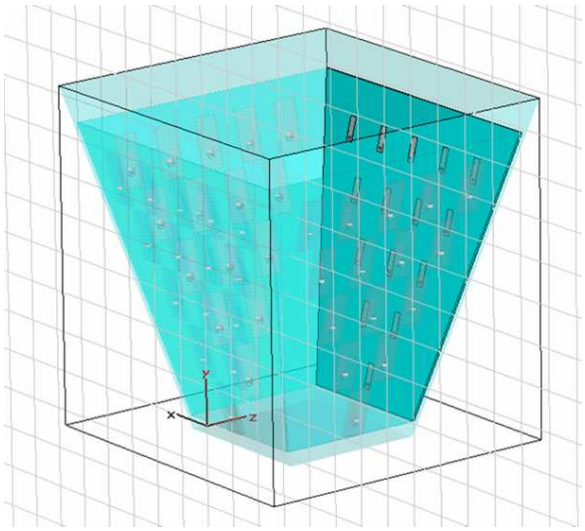

Figure 18: Imaging chamber for proposed high frequency 3-D microwave imaging system.

used instead of the more complex folded patch antennas. Additionally, the use of simple patch antennas will simplify the task of modeling the imaging system for image reconstruction. Finally, new M/A-Com SW90-0004A RF switches will be used to reduce losses due to the multiplexers had the new higher operating frequency.

8 Acknowledgments

The author would like to thank his advisor Prof. Gary A. Ybarra, Prof. Qing H. Liu, Prof. William T. Joines, Prof. Rhett George, John P. Stang and Jack Skinner for their assistance and guidance on this project. This research was funded in part by the National Institutes of Health under the NCI grant 5R01CA102768-02.

References

[1] Breast cancer symptoms and information on breast cancer. Technical report, National Breast Cancer Foundation, Inc., April 2005. Retrieved April 18, 2005 from http://www.nationalbreastcancer.org/early_detection/index.html.

[2] Cancer facts & figures 2005. Technical report, American Cancer Society, 2005. Retrieved March 23, 2006 from http://www.cancer.org/downloads/STT/CAFF2005BrF.pdf.

[3] Qing Huo Liu, Zhong Qing Zhang, Tonghui T. Wang, J. A. Bryan, Gary A. Ybarra, Loren W. Nolte, and William T. Joines. Active microwave imaging–2-d forward and inverse scattering methods. *IEEE Transactions on Microwave Theory And Techniques*, 50(1):123–133, January 2002.

[4] Qing Huo Liu. A short tutorial on 3d microwave imaging system for breast cancer detection. Retrieved April 26, 2006 from http://mwi.pratt.duke.edu/Resources/mwi.pdf, 2004.

[5] Zhong Qing Zhang, Qing Huo Liu, Chunjiang Xiao, Erika Ward, Gary Ybarra, and William T. Joines. Microwave breast imaging: 3-d forward scattering simulation. *IEEE Transactions on Biomedical Engineering*, 50:1180–1189, October 2003.